Original Article

Deciphering immune landscapes: an ICD-lncRNA-derived prognostic signature for pancreatic adenocarcinoma

Hao Zhu, Xiaojie Gan, Danyang Shen, Ding Sun

Department of General Surgery, The First Affiliated Hospital of Soochow University, Suzhou, China

Contributions: (I) Conception and design: H Zhu; (II) Administrative support: D Shen, D Sun; (III) Provision of study materials or patients: D Shen, D Sun; (IV) Collection and assembly of data: H Zhu, X Gan; (V) Data analysis and interpretation: H Zhu, D Shen; (VI) Manuscript writing: All authors; (VII) Final approval of manuscript: All authors.

Correspondence to: Ding Sun, MD; Danyang Shen, MD. Department of General Surgery, The First Affiliated Hospital of Soochow University, 899 Pinghai Road, Gusu District, Suzhou 215006, China. Email: sunding@suda.edu.cn; shendanyang@suda.edu.cn.

Background: In recent years, immunogenic cell death (ICD) and long non-coding RNAs (lncRNAs) have been implicated in tumor invasion and growth. However, the role of ICD-associated lncRNAs in pancreatic adenocarcinoma (PAAD) remains unclear. Therefore, this study aimed to develop and validate a prognostic signature based on ICD-associated lncRNAs for PAAD patients and to explore its potential associations with immune processes.

Methods: We identified ICD-associated genes from the GeneCards database and obtained transcriptomic data and sample information for PAAD from The Cancer Genome Atlas (TCGA). Using these datasets, we primarily aimed to develop and validate a prognostic signature based on ICD-associated lncRNAs. A prognostic signature and nomogram were constructed to predict patient outcomes. To preliminarily explore potential underlying mechanisms related to immunity, we performed enrichment analysis [Gene Ontology (GO)/Kyoto Encyclopedia of Genes and Genomes (KEGG)], tumor mutational burden (TMB) assessment, comprehensive immune correlate analysis, and pharmacosensitivity profiling. Additionally, to explore the functional role of a key lncRNA (LINC00705) in PAAD, we modulated its expression in PANC-1 and MIAPaCa-2 cell lines through knockdown and overexpression strategies.

Results: We identified six ICD-associated lncRNAs (ZEB2-AS1, AC099792.1, LINC01091, LINC02613, AC005304.3, and LINC00705) and constructed a prognostic signature. Survival analyses, univariate and multivariate Cox regression, and receiver operating characteristic (ROC) curve analysis and dynamic nomogram demonstrated the robust accuracy of this six-lncRNA signature in predicting PAAD patient prognosis. Pathway enrichment analysis of the low-risk cohort suggested a potential link to immune-related processes, providing preliminary insights into possible mechanisms. Patients exhibiting a higher risk score were significantly associated with elevated TMB (P=0.001). Immune-related analyses of the low-risk cohort revealed higher immune cell infiltration, improved immune function scores, and elevated expression of immune checkpoints. Pharmacosensitivity profiling identified 15 drugs with differential sensitivity. *In vitro* experiments showed that LINC00705 significantly affected the biological behaviors of pancreatic cancer cells.

Conclusions: We developed and validated a prognostic signature based on six ICD-associated lncRNAs, demonstrating its significant accuracy in predicting outcomes for PAAD patients. This signature holds potential for providing more precise clinical guidance. Furthermore, our preliminary bioinformatic analyses suggest associations between the signature and immune processes, warranting future mechanistic investigation. Additionally, modulating LINC00705 expression may offer a promising strategy to inhibit cancer cell growth and metastasis.

Keywords: Pancreatic adenocarcinoma (PAAD); immunogenic cell death (ICD); long non-coding RNAs (lncRNAs); immune; prognostic signature

Copyright © 2025 AME Publishing Company. All rights reserved.

Submitted Mar 14, 2025. Accepted for publication Jul 29, 2025. Published online Oct 29, 2025.
doi: 10.21037/tcr-2025-582
View this article at: https://dx.doi.org/10.21037/tcr-2025-582

Introduction

Pancreatic adenocarcinoma (PAAD) is an aggressive malignancy of the digestive system with a dismal prognosis, and it contributes significantly to the global tally of cancer-related deaths (1). According to estimates, approximately 128,000 individuals in Europe succumb to PAAD annually (2). Due to late-stage diagnosis, when surgical options are often no longer feasible, the median survival time is less than a year (3). Pancreaticoduodenectomy remains the mainstay of treatment for PAAD (4). However, even with combined surgical and chemotherapy treatments, the long-term survival rate at 5 years only modestly increases from 5% to 25% (5). During the last few years, immunotherapy has gained prominence as a key therapeutic approach in oncology. This approach activates the body's immune system, thereby disrupting the advancement and systemic spread of malignancies. Monoclonal antibodies targeting programmed cell death protein-1 (PD-1) and cytotoxic T-lymphocyte-associated antigen 4 (CTLA-4) to modulate immune checkpoint pathways have shown promising results in inhibiting tumor progression. These effective strategies have revolutionized cancer treatment (6). Nevertheless, precise prognosis prediction in PAAD remains challenged by high intertumoral heterogeneity and scarce validated biomarkers, with over 40% of resected patients recurring within 12 months (1). Immunotherapy achieves less than 10% response rates in PAAD due to its profoundly immunosuppressive tumor microenvironment (TME) characterized by dense fibrosis, deficient T-cell infiltration, and abundant immunosuppressive cells (7). Therefore, discovering biomarkers that can predict individual patient outcomes and serve as targets for immunotherapeutic interventions is crucial for advancing PAAD treatment strategies.

Immunogenic cell death (ICD) refers to a regulated form of cellular demise triggered by a range of therapeutic approaches, including pharmacological chemotherapy, physical and chemical therapies, and photodynamic therapy (8). During the ICD process, a variety of damage-associated molecular patterns (DAMPs), such as adenosine triphosphate (ATP), troponin, and type I interferons (IFNs), are released through active secretion or passive diffusion. These DAMPs act as "trigger points" for immune response activation, engaging with specific pattern recognition receptors (PRRs) found on dendritic cells (DCs). This initiates a molecular cascade that orchestrates the innate and learned immune response systems to target tumor cells, eliciting a specific anti-tumor response (9-11). Additionally, ICD enhances immune responses within the TME by promoting the aggregation and activation of antigen-presenting cells (12). While ICD induction combined with checkpoint inhibitors (e.g., anti-PD-1 antibodies) has shown encouraging outcomes in breast cancer and small cell lung cancer (13,14), its broader application faces two fundamental challenges. On one hand, reliable biomarkers for predicting ICD efficacy across diverse tumor types remain elusive, limiting clinical translation. On the other hand, current ICD strategies predominantly rely on external stimuli like chemotherapy or radiation, overlooking endogenous regulators such as lncRNAs that may orchestrate ICD pathways. Therefore, therapeutic strategies inducing ICD to suppress tumor progression require deeper investigation.

Highlight box

Key findings

- This study identified a six-immunogenic cell death (ICD)-associated long non-coding RNA (lncRNA) prognostic signature for pancreatic adenocarcinoma (PAAD), demonstrating its predictive value for survival, immune infiltration, and therapy response. Experimental validation highlighted LINC00705 as a functional regulator of pancreatic cancer cell behavior, suggesting its therapeutic potential.

What is known and what is new?

- In recent years, ICD and lncRNAs have been implicated in tumor invasion and growth. However, the role of ICD-associated lncRNAs in PAAD remains unclear.
- The identification of ICD-associated lncRNAs as biomarkers in PAAD patients holds significant prognostic value. LINC00705 expression may offer a promising strategy to inhibit cancer cell growth and metastasis.

What is the implication, and what should change now?

- LINC00705 may serve as both a predictive biomarker for immunotherapy response and a potential therapeutic target in PAAD patients.

Copyright © 2025 AME Publishing Company. All rights reserved.

Long non-coding RNAs (lncRNAs), which are RNA molecules longer than 200 nucleotides and devoid of protein-coding capacity, constitute a crucial category of functional elements within the genome (15). These molecules are involved in a wide array of cellular processes such as metabolism, cell cycle regulation, and differentiation by interacting with DNA and other RNA molecules, thereby modulating protein/RNA stability, transcription, translation, and post-translational modifications (16,17). Furthermore, lncRNAs have been implicated in regulating cancer progression by targeting specific signaling cascades (18). For example, the lncRNA DUXAP8 has been shown to enhance the aggressiveness and metastatic potential of pancreatic cancer through the miR-448/WTAP/Fak signaling pathway (19). Currently, lncRNA-based signatures associated with ICD have demonstrated high predictive accuracy in several malignancies—notably a thyroid cancer signature by Wang *et al.* [area under the curve (AUC) =0.811] and an ICD-related lncRNA model in lung cancer developed by Shu *et al.* (AUC =0.727) (20,21). However, two critical gaps impede progress: most existing lncRNA signatures lack experimental validation of their immune-modulatory functions, and the potential crosstalk between ICD pathways and lncRNA networks in PAAD remains completely unexplored.

In this study, we leveraged PAAD transcriptomic data from The Cancer Genome Atlas (TCGA) database to identify ICD-associated lncRNAs and construct a prognostic signature. Our work aimed to rigorously establish the predictive accuracy of this signature for PAAD patient outcomes. Employing a comprehensive suite of bioinformatics methods, we identified six lncRNAs and constructed the prognostic model. Subsequently, we divided PAAD patients into risk cohorts based on the signature and performed extensive validation analyses, including survival assessment, receiver operating characteristic (ROC) curve evaluation, and Cox regression modeling, to quantify its prognostic power. Furthermore, to explore the biological relevance and potential immune mechanisms underpinning the signature, we characterized the identified risk subgroups in terms of tumor mutational burden (TMB), immune cell infiltration, immune checkpoint modulation, and drug responsiveness, and conducted pathway enrichment analysis [Gene Ontology (GO)/Kyoto Encyclopedia of Genes and Genomes (KEGG)]. Finally, to functionally investigate a key component of the signature, we performed *in vitro* experiments to assess the effects of LINC00705 on pancreatic cancer cell behaviors. We present this article in accordance with the TRIPOD and MDAR reporting checklists (available at https://tcr.amegroups.com/article/view/10.21037/tcr-2025-582/rc).

Methods

Data collection

We accessed the GeneCards database (https://www.genecards.org/) and identified 177 genes associated with ICD with a score greater than 35. Transcriptome expression profiles, single nucleotide mutation data, clinical characteristic data, and survival information for patients diagnosed with PAAD were retrieved from TCGA (https://portal.gdc.cancer.gov/). Among the 185 samples, 181 were tumor tissues and 4 were normal tissues. After excluding 3 samples lacking survival information, the remaining samples were allocated into the training and testing sets through random assignment, with an equal distribution maintained at a 1:1 ratio. The study was conducted in accordance with the Declaration of Helsinki and its subsequent amendments. Ethical approval was obtained from the Ethics Committee of the First Affiliated Hospital of Soochow University (No. 2025742). Informed consent was exempted as all patient data were derived from deidentified public databases where original ethical compliance had been established. Clinical data for patients in each cohort are presented in *Table 1*. *Figure 1* illustrates the data processing workflow.

Identification of ICD-associated lncRNA and construction of a prognostic signature

To examine lncRNAs significantly associated with ICD, Pearson correlation analysis was performed with a threshold of |correlation coefficient| >0.3 and P<0.001. Subsequently, differential expression analysis (22) was conducted to identify lncRNAs with differential expression between tumor and normal samples [ICD-related differentially expressed lncRNAs (DElncRNAs), $|\log_2$fold change (FC)| >1, P<0.05]. To enhance the overall performance of the prognostic signature in predicting outcomes for PAAD, a series of algorithmic combinations was performed using survival information from the training cohort. These procedures encompassed univariate Cox regression, least absolute shrinkage and selection operator (LASSO) analysis, followed by multivariate Cox regression. This process culminated in the identification of six ICD-associated lncRNAs. Ultimately, the prognostic signature was

Copyright © 2025 AME Publishing Company. All rights reserved.

Table 1 Clinical information of PAAD patients in the training, test, and entire groups

Feature	Train (n=89), n (%)	Test (n=89), n (%)	Entire (n=178), n (%)
Age (years)			
<65	38 (42.7)	44 (49.4)	82 (46.1)
≥65	51 (53.7)	45 (50.6)	96 (53.9)
Gender			
Female	40 (44.9)	40 (44.9)	80 (44.9)
Male	49 (55.1)	49 (55.1)	98 (55.1)
Stage			
Stage I	11 (12.4)	10 (11.2)	21 (11.8)
Stage II	72 (80.9)	75 (84.4)	147 (82.6)
Stage III	2 (2.2)	1 (1.1)	3 (1.7)
Stage IV	3 (3.4)	1 (1.1)	4 (2.2)
Unknown	1 (1.1)	2 (2.2)	3 (1.7)
T			
T1	4 (4.5)	3 (3.4)	7 (3.9)
T2	10 (11.2)	14 (15.7)	24 (13.5)
T3	72 (81)	70 (78.7)	142 (79.8)
T4	2 (2.2)	1 (1.1)	3 (1.7)
Unknown	1 (1.1)	1 (1.1)	2 (1.1)
N			
N0	34 (38.2)	15 (16.9)	49 (27.5)
N1	53 (59.6)	71 (79.7)	124 (69.7)
Unknown	2 (2.2)	3 (3.4)	5 (2.8)
Status			
Alive	42 (47.2)	43 (48.3)	85 (47.8)
Dead	47 (52.8)	46 (51.7)	93 (52.2)

N, node; PAAD, pancreatic adenocarcinoma; T, tumor.

developed by integrating expression levels and correlation coefficients across various samples, with the formula as follows: risk score = (genecoef1 × gene1 expression) + (genecoef2 × gene2 expression) +…+ (genecoefN × geneN expression).

Evaluation of the prognostic signature's predictive performance

The optimal cutoff point for classifying PAAD patients into high- and low-risk groups was determined using the median risk score (20). Survival analysis was performed on three cohorts using Kaplan-Meier curves to assess the correlation between risk scores and patient survival time. The accuracy of the predictive model across these cohorts was evaluated by calculating the AUC for ROC (23) at 1-, 3-, and 5-year time points using the "timeROC" package. Survival analyses were then performed within subgroups defined by different clinical features to assess the generalizability of our model algorithm.

Exploring the clinical significance of predictive model

Univariate and multivariate Cox regression analyses (24), commonly used to assess the impact of multiple variables on a certain outcome, were performed to evaluate the independence of the risk scores derived from the predictive model. The univariate analysis first assessed the individual effect of each factor on survival, including age, gender, tumor staging, tumor (T)-stage, and node (N)-stage. The multivariate analysis, which accounts for the potential interrelationships between these variables, was then applied to evaluate whether the calculated risk scores remained an independent prognostic factor. A nomogram (25) for PAAD was then developed utilizing the 'nomogramEx' package, allowing for a more objective estimation of patient survival at various time points based on these clinical factors. ROC curves were generated for the risk scores and various clinical features, with the AUC calculated and compared to evaluate their respective predictive capabilities for patient outcomes. Calibration curves (26) were plotted to visualize the agreement between observed survival outcomes and the probabilities estimated by the nomogram. The accuracy of the nomogram in predicting patient survival probabilities was assessed by examining the fit of these calibration curves.

Enrichment analysis

In order to gain a deeper understanding of the underlying mechanisms of gene function in biology, GO and KEGG pathway analyses (27) were performed on genes that were differentially expressed between the high- and low-risk patient groups. Enrichment was deemed significant if false discovery rate (FDR) and $P<0.05$. Subsequently, genes were ranked based on their differential expression levels across two risk cohorts. Gene set enrichment analysis (GSEA) (28) was then conducted using the KEGG gene sets to identify pathways enriched at the top or bottom of the risk groups.

Copyright © 2025 AME Publishing Company. All rights reserved.

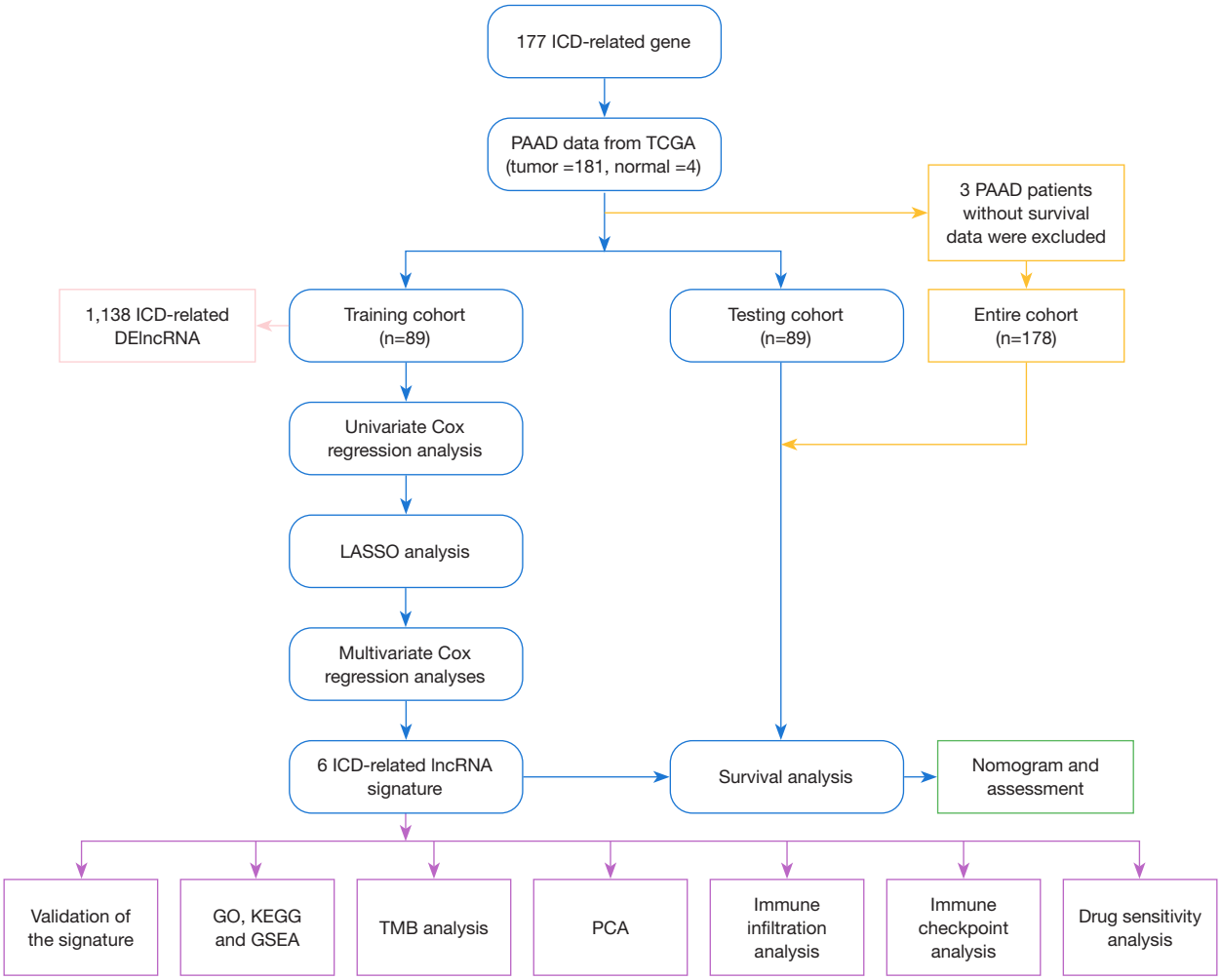


Figure 1 Study flowchart. DElncRNA, differentially expressed lncRNAs; GO, Gene Ontology; GSEA, gene set enrichment analysis; ICD, immunogenic cell death; KEGG, Kyoto Encyclopedia of Genes and Genomes; LASSO, least absolute shrinkage and selection operator; lncRNA, long non-coding RNAs; PAAD, pancreatic adenocarcinoma; PCA, principal component analysis; TCGA, The Cancer Genome Atlas; TMB, tumor mutational burden.

Mutation analysis of DElncRNAs

The TMB (29) score for each PAAD sample was calculated. To identify somatic mutations that distinguish low-risk and high-risk populations, we used box plots to visualize mutational differences among PAAD patients. A waterfall plot displaying the mutational profiles of both groups was generated using the 'maftools' package. Finally, Kaplan-Meier survival analysis was performed on high- and low-TMB, and risk score-defined subgroups to investigate the potential prognostic impact of TMB in combination with risk scores.

Principal component analysis (PCA)

We employed the 'scatterplot3d' package in R to perform PCA (30) on the ICD genes, all lncRNAs, ICD-related DElncRNAs, and the six ICD-related lncRNAs.

Immune cell infiltration and immune checkpoint analysis

Single-sample gene set enrichment analysis (ssGSEA) (31), an extension of traditional GSEA, was applied for analyzing individual gene expression samples, inferring the enrichment levels of gene sets within each sample. This

Copyright © 2025 AME Publishing Company. All rights reserved.

approach was used to compare differences in immune cells and immune regulatory mechanisms between the two risk groups. Furthermore, the CIBERSORT algorithm (31), which relies on gene expression data and a specific immune cell signature matrix, calculates the fraction of immune cells infiltrating the tumor by detecting the expression of marker genes. We employed this algorithm for immune infiltration analysis and to plot scatter plots correlating risk scores with various immune cells. Finally, based on known immune checkpoint information, we used the 'reshape2' package to conduct a comparative analysis of immune checkpoints between the two risk groups.

Exploration of chemotherapeutic drugs for PAAD in clinical settings

The responsiveness of the two risk groups to chemotherapeutic agents was assessed based on half-maximal inhibitory concentration (IC_{50}) values. We selected 138 compounds from the Genomics of Drug Sensitivity in Cancer database (GDSC, release 8.4), encompassing FDA-approved and clinically trialed oncology drugs. Sensitivity was evaluated using statistically significant inter-group IC_{50} differences ($P<0.05$), where lower IC_{50} values indicated higher drug sensitivity. This analysis identified potential therapeutic agents for PAAD patients stratified by the ICD-lncRNA-derived risk signature.

Mechanistic prediction of LINC00705 regulatory networks

To elucidate the molecular mechanisms underlying LINC00705-mediated regulation, potential miRNA interactors were screened using three independent prediction software tools under stringent criteria: miRanda (version 3.3a) required a sequence complementarity score ≥140 and minimum free energy (MFE) ≤−15 kcal/mol; RNAhybrid (version 2.1.2) applied an MFE threshold of ≤−15 kcal/mol ($P<0.05$); and Predicted Interaction Targets from Array and Annotations (PITA) (version 6) used a binding energy cutoff of ≤−10 kcal/mol. High-confidence miRNA candidates were defined as those predicted by all three tools. Experimentally validated miRNA-mRNA interactions were extracted from the Encyclopedia of RNA Interactomes (ENCORI) database (2023-01 release), with target verification performed using its integrated computational modules (microT-CDS, miRmap, PITA, and TargetScan). Consensus target genes were identified through Venn analysis using the R package VennDiagram (version 1.7.3), followed by KEGG pathway enrichment analysis with clusterProfiler (version 4.0) at an adjusted P value threshold of <0.05.

Cultivation of pancreatic cancer cells

PANC-1 and MIAPaCa-2 cells (sourced from Zhongqiao Xinzhou Biotechnology Co., Ltd., Shanghai, China) were cultivated in DMEM/F12 medium (Gibco, New York, USA) supplemented with 10% fetal bovine serum and 100 U/mL penicillin/streptomycin solution. The cellular cultures were placed in an incubator set at 37 ℃ and supplied with 5% CO_2 for optimal growth conditions.

LINC00705 cell transfection

The LINC00705 overexpression plasmid was designed and custom-made by Suzhou Jima Gene Co. Ltd. (Suzhou, China). The siRNA targeting LINC00705 was manufactured by Siran Biotech Co., Ltd. (Suzhou, China). When the two types of PAAD cells reached 70% confluence, the LINC00705 overexpression plasmid and siRNA were transfected into the two types of PAAD cells separately with Lipofectamine 3000 (Invitrogen, Shanghai, China), following the recommended protocol.

Quantitative polymerase chain reaction (qPCR)

Total RNA was extracted from transfected MIAPaCa-2 and PANC-1 cells using Trizol reagent (Beyotime, Shanghai, China). Subsequently, complementary DNA (cDNA) was synthesized using SuperScript II reverse transcriptase (Thermo Fisher Scientific, Carlsbad, USA). qPCR was performed using a mixture containing cDNA template, SYBR Green I mix, and custom-specific primers for the LINC00705 gene. The GAPDH gene served as the endogenous standard for data normalization, primer information is shown in Table S1. The qPCR MIX from ABClonal (Wuhan, China) was employed, and each experiment was performed in triplicate. The expression levels of the LINC00705 gene were graphically represented as bar charts using GraphPad Prism software (version 9.5.1).

Cell Counting Kit-8 (CCK-8) assay

Forty-eight hours post-transfection, PANC-1 and MIAPaCa-2 cells were individually seeded into 96-well plates at a density of 2,000 cells per well. To reduce experimental

Copyright © 2025 AME Publishing Company. All rights reserved.

variability, three replicate wells were established for each cell group. The cells were then cultured for 12 hours until they were fully adherent. Subsequently, at 0, 24, 48, 72, and 96 h time points, 10 µL of CCK-8 solution was added to 90 µL of DMEM in each well. The plates were incubated for an additional 3 hours. An automated plate reader was then utilized to measure the absorbance at 450 nm, thereby determining the optical density (OD) values. These OD values were used to assess the proliferation kinetics of the cells over the specified time intervals.

Transwell assay

Firstly, 50 µL of Matrigel matrix solution was added to the upper chamber of each Transwell well to establish the invasion experimental environment. The upper compartment without Matrigel matrix solution was used to create the migration experimental environment. A cell suspension of 2×10^5 cells/mL was formulated using serum-free Dulbecco's Modified Eagle's Medium (DMEM) and subsequently introduced into the upper compartment of each well. DMEM complete medium containing 10% fetal bovine serum (FBS) was added to the lower compartment. After 24 hours of culture, the non-invaded cells on the upper surface of the membrane were carefully removed using a cotton swab. The cells that had invaded through the membrane to the lower surface were then fixed with 4% paraformaldehyde for 30 minutes, followed by staining with 0.1% crystal violet solution for 10 minutes at room temperature. After staining, the membranes were rinsed thoroughly with phosphate-buffered saline (PBS) until the background was clear, and were air-dried. The stained cells on the membrane were then imaged under a microscope. The cell counting was performed with ImageJ.

5-ethynyl-2'-deoxyuridine (EdU) immunofluorescence

The EdU assay kit (ApexBio, USA) was employed to stain proliferating cells. PANC-1 and MIAPaCa-2 cells were seeded into a 24-well plate at a density of 3×10^4 cells per well and incubated at 37 ℃ for 12 hours to facilitate adhesion. A working solution of EdU at a concentration of 10 µM was added to each well. The plate was then returned to the incubator at 37 ℃ for an additional 2 hours to allow for the incorporation of EdU into newly synthesized cellular DNA. Subsequently, the cells were fixed with a 4% paraformaldehyde solution for 30 minutes, followed by permeabilization with a 0.5% Triton X-100 in PBS solution for 15 minutes to enhance membrane permeability. The fluorescent labeling reaction was initiated by adding solution to each well and incubating in the dark at room temperature for 30 minutes, followed by the addition of diamidino-2-phenylindole (DAPI) solution and a further 10-minute incubation in darkness. The cell proliferation was assessed by counting EdU-positive cells with ImageJ software.

Wound scratch assay

When the two cell lines were cultured to full confluence, a straight-line scratch was meticulously created within the monolayer using a sterile 200 µL pipette tip, resulting in a clearly delineated wound region. Following this, the cells underwent gentle washing with PBS buffer to remove any cellular debris. The culture medium was replaced with DMEM supplemented with 1% FBS to minimize cell proliferation, which could potentially reduce the wound area. Subsequently, the cells were placed in the incubator to continue growing. Images of the wound area were captured using a microscope at 0 and 24 hours post-wounding.

Statistical analysis

All statistical analyses were conducted utilizing R software (Version 4.4.3). A P value threshold of less than 0.05 was considered indicative of statistical significance.

Results

Establishment of a prognostic signature for patients with PAAD

Pearson correlation analysis and differential expression analysis were initially performed among 177 ICD-related genes and 16,832 lncRNAs. A rigorous screening process identified 1,138 ICD-related DElncRNAs, with 162 showing upregulation and 976 exhibiting downregulation (*Figure 2A*). Among the 178 PAAD cases with available prognostic data, a balanced 1:1 ratio was maintained to randomly assign them to training and testing cohorts (*Table 1*). Univariate Cox analysis (P<0.05) identified 89 promising ICD-related lncRNAs. Subsequently, LASSO regression analysis was conducted, leading to the selection of 29 ICD-related lncRNAs (*Figure 2B*,*2C*). To enhance the precision of the selected lncRNAs in constructing a prognostic signature, multivariate Cox analysis was further employed, ultimately

Copyright © 2025 AME Publishing Company. All rights reserved.

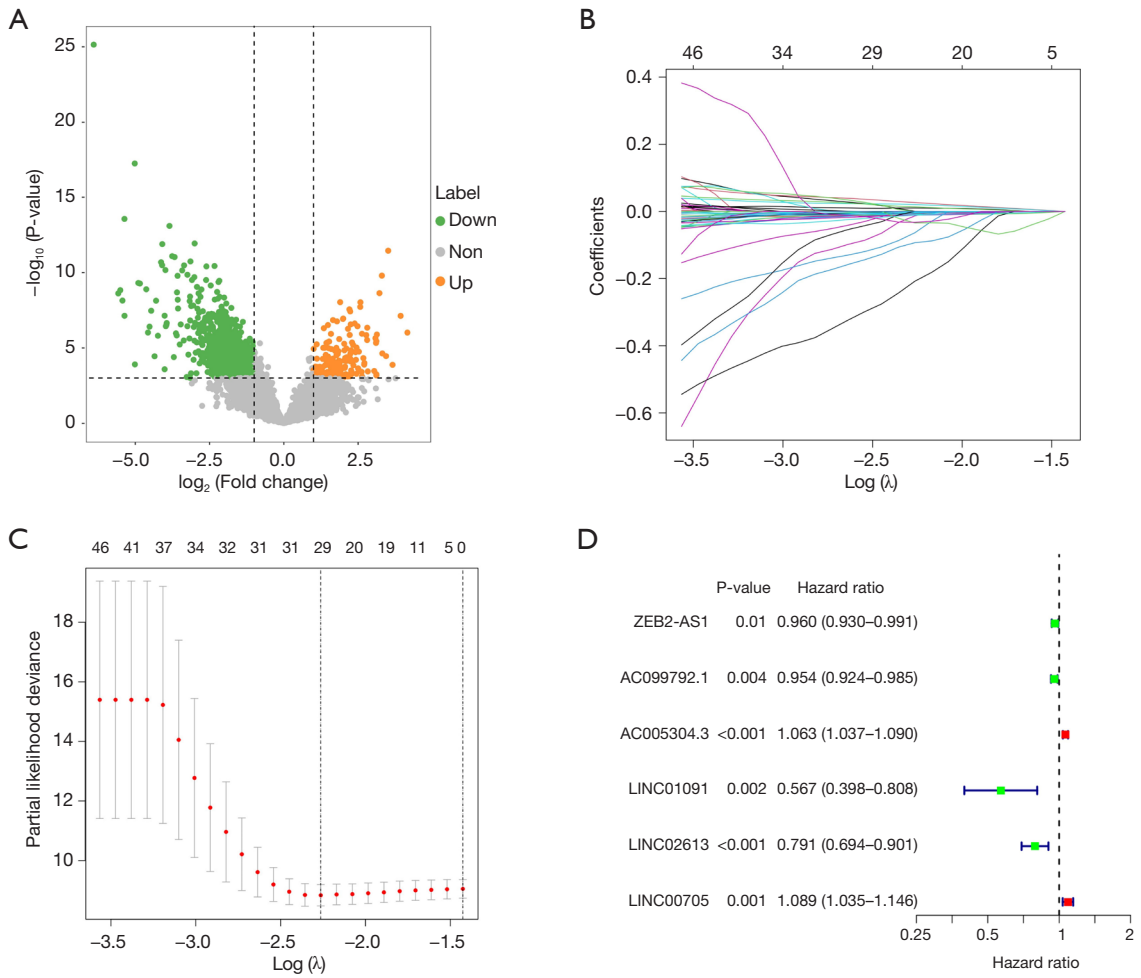


Figure 2 Selection of ICD-related lncRNAs for constructing a PAAD prognosis model. (A) Volcano plot of differentially expressed lncRNAs in PAAD tumor versus normal tissues. (B) LASSO coefficient distribution for 29 ICD-lncRNAs associated with prognosis. (C) Cross-validation using LASSO regression analysis. (D) Six ICD-lncRNAs selected for building the prediction model after multivariable Cox regression analysis. Red blocks indicate risk factors (HR >1), while green blocks denote protective factors (HR <1) for prognosis. HR, hazard ratio; ICD, immunogenic cell death; LASSO, least absolute shrinkage and selection operator; lncRNA, long non-coding RNAs; PAAD, pancreatic adenocarcinoma.

identifying four ICD-related lncRNAs with a protective effect on prognosis (ZEB2-AS1, AC099792.1, LINC01091, LINC02613) and two other lncRNAs as risk factors for poor prognosis (AC005304.3, LINC00705) (*Figure 2D*). A prognostic prediction model for PAAD was constructed based on the six ICD-associated lncRNAs. The following formula was used to calculate the risk score for each patient:

Risk score = (−0.040488881 × ZEB2AS1 expression) + (−0.234536765 × LINC02613 expression) + (−0.567345443 × LINC01091 expression) + (−0.047316955 × AC099792.1 expression) + (0.061493333 × AC005304.3 expression) + (0.085203143 × LINC00705 expression). After calculating the risk scores, the cohort of 178 patients was stratified into high- (n=89) and low-risk (n=89) groups.

Validation of the predictive performance of the signature

To rigorously validate the stability and effectiveness of the signature, extensive confirmatory analyses were conducted from various aspects. Survival analysis using Kaplan-Meier curves across the training, testing, and entire cohorts demonstrated that individuals in the high-risk group showed markedly poorer overall survival (OS) than those in the low-risk group (*Figure 3A-3C*). Moreover, the areas

Copyright © 2025 AME Publishing Company. All rights reserved.

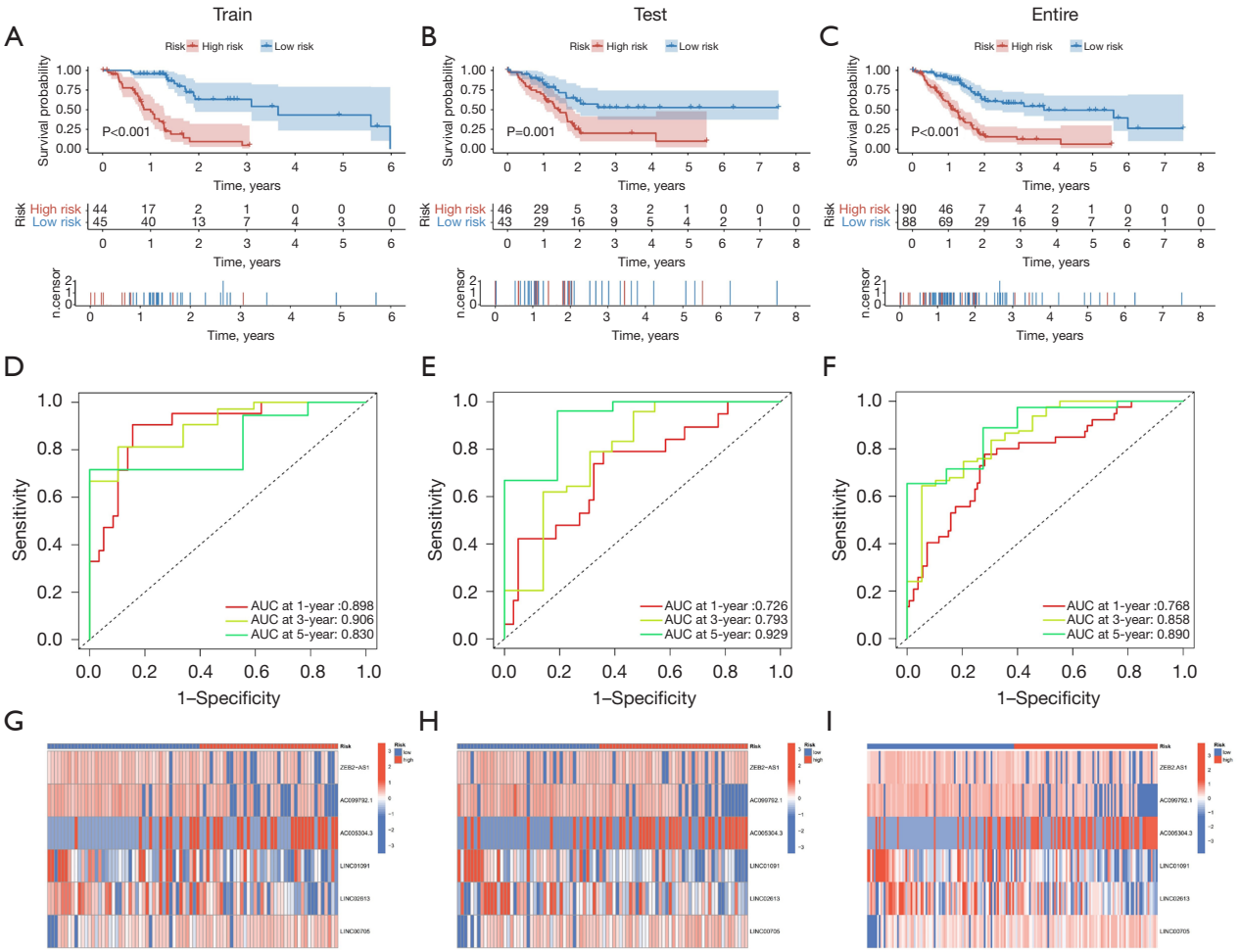


Figure 3 Validation and evaluation of the PAAD prognosis model. (A-C) Kaplan-Meier survival curves for high- and low-risk PAAD patients in the training cohort (A), validation cohort (B), and entire cohort (C). (D-F) Time-dependent ROC curves evaluating prediction accuracy in the training set (D), test set (E), and combined cohort (F). (G-I) Expression heatmaps of six prognostic lncRNAs across training (G), test (H), and full cohorts (I). AUC, area under the curve; PAAD, pancreatic adenocarcinoma; ROC, receiver operating characteristic.

under the time-dependent ROC curves for the 1-, 3-, and 5-year OS predictions of the signature confirmed its robust predictive capacity (training cohort 1-, 3-, 5-year AUC: 0.898, 0.906, 0.830; testing cohort 1-, 3-, 5-year AUC: 0.726, 0.793, 0.929; entire cohort: 1-, 3-, 5-year AUC: 0.768, 0.858, 0.890) (*Figure 3D-3F*). The distribution of risk scores across the three cohorts (Figure S1A-S1C), coupled with the scatter plots reflecting patient survival status (Figure S1D-S1F), indicated that the low-risk group predominantly enjoyed more favorable prognoses. The consistency of these findings across cohorts attests to the robust fit of the signature. The expression heatmaps of the six lncRNAs revealed that AC005304.3 and LINC00705 were predominantly highly expressed, while ZEB2-AS1, AC099792.1, LINC01091, and LINC02613 were predominantly lowly expressed within tumor samples (*Figure 3G-3I*), corroborating the findings from the multivariate analysis (*Figure 2D*). PCA demonstrated that, after a series of screenings, the six ICD-associated lncRNAs effectively discriminated between the two risk subgroups, resulting in a clear separation between the groups (Figure S2A-S2D). Finally, KM analysis was conducted across various clinical subgroups (Figure S3A-S3J). Except for the limited number of stage III–IV patients, which did not allow for a true reflection of the situation, the consistency of the results indicated that high-risk score patients experienced a substantially dismal prognosis across all clinical subgroups, suggesting the broad applicability of this predictive model.

Copyright © 2025 AME Publishing Company. All rights reserved.

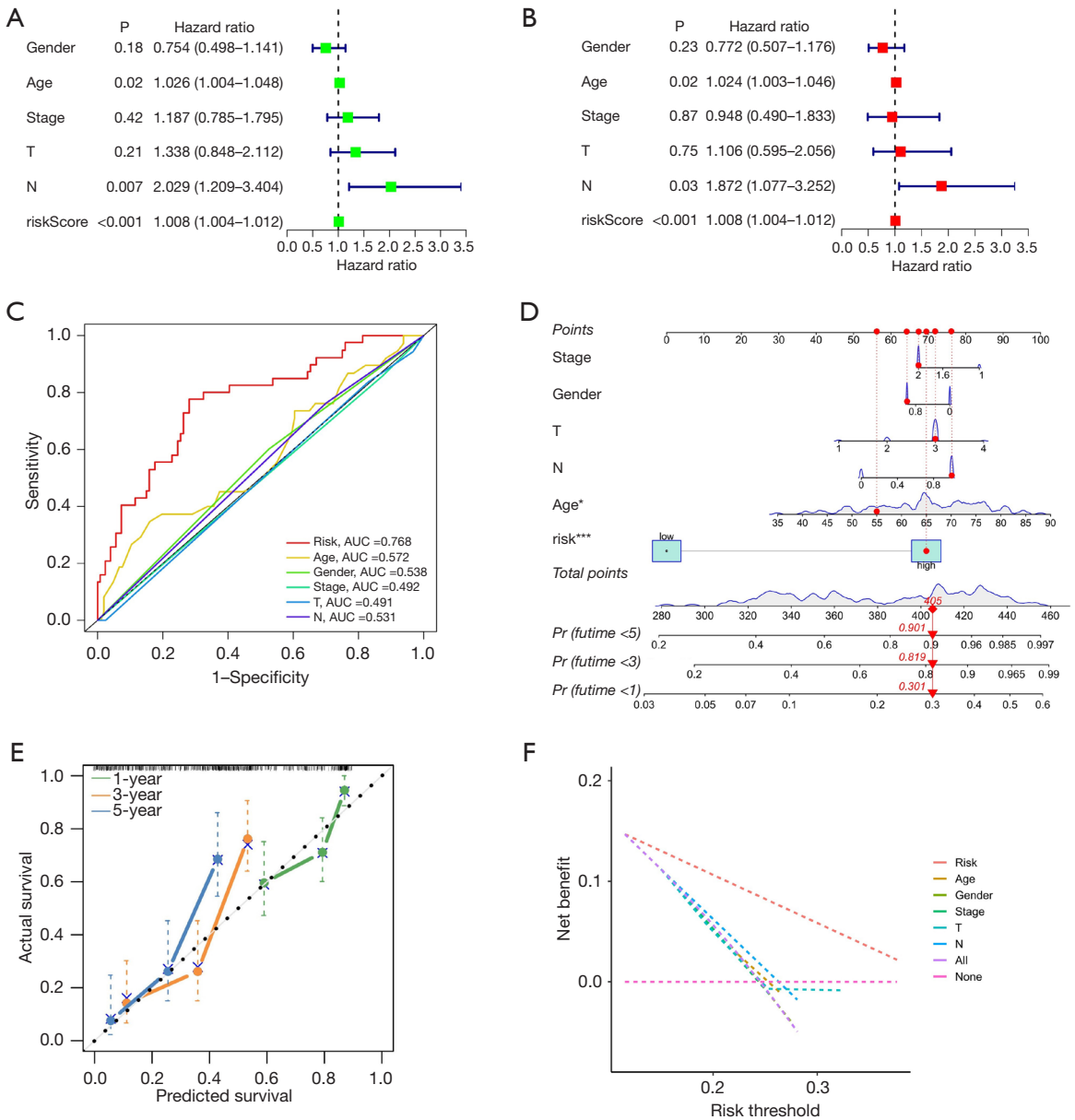


Figure 4 Clinical value of the prediction model. (A,B) Univariate and multivariate Cox regression analysis of six factors associated with prognosis. (C) ROC curves reflecting the predictive accuracy of five clinical characteristics and risk scores. (D) Dynamic nomogram integrating risk scores with gender, age, stage, T, and N to predict the OS of PAAD patients. (E) Calibration curves for survival rate prediction. (F) Decision curve for risk scores and five clinical characteristics. *, P<0.05; ***, P<0.001. AUC, area under the curve; N, node; OS, overall survival; PAAD, pancreatic adenocarcinoma; ROC, receiver operating characteristic; T, tumor.

Clinical significance of the predictive models

We performed a comprehensive set of algorithmic analyses to evaluate the accuracy of the risk scores calculated by the predictive model in actual clinical applications. Initially, univariate and multivariate analyses identified N staging and risk scores as independent predictors of OS in patients (*Figure 4A*,*4B*). The other variables did not exhibit significant correlations. ROC curves for patient clinical characteristics and risk scores demonstrated that the risk scores had a significantly higher predictive power compared

Copyright © 2025 AME Publishing Company. All rights reserved.

to other factors (*Figure 4C*). To offer a more straightforward and visual tool for estimating the 1-, 3-, and 5-year survival rates of patients, a dynamic nomogram was developed that integrated these characteristics (*Figure 4D*). The calibration curve showed that this Nomogram was highly accurate in forecasting survival probabilities (*Figure 4E*). Furthermore, decision curve analysis (DCA) confirmed that the risk score significantly contributed to improving the predictive accuracy of the survival model (*Figure 4F*).

Enrichment analysis to explore the biological significance of genes

To gain deeper insight into the functional mechanisms driving pancreatic cancer progression, we conducted functional enrichment analysis on the genes that were differentially expressed between the two risk subgroups, with the majority being downregulated (*Figure 5A*). As depicted in *Figure 5B*, GO analysis indicated that the top three biological processes were regulation of membrane potential, signal release and modulation of chemical synaptic transmission. In the cellular component category, the highest enrichment levels were detected in the neuronal cell body, synaptic membrane, and transporter complex. Regarding molecular function, the differentially expressed genes were notably enriched in monoatomic ion channel activity, metal ion transmembrane transporter activity, and monoatomic ion-gated channel activity. KEGG pathway analysis of these genes revealed significant enrichment in pathways such as neuroactive ligand-receptor interaction, cyclic adenosine monophosphate (cAMP) signaling pathway, and retrograde endocannabinoid signaling (*Figure 5C*). Subsequent GSEA highlighted significant enrichment in the high-risk group for processes including folate transport and metabolism, NF-κB signaling pathway and systemic lupus erythematosus (*Figure 5D*). Conversely, the low-risk group exhibited predominant enrichment in amphetamine addiction, dopaminergic synapse, nicotine addiction, Parkinson's disease, and pathways associated with neurodegeneration across multiple diseases (*Figure 5E*). This comprehensive suite of enrichment analyses from various perspectives underscores the substantial involvement of differentially expressed genes in the progression of PAAD through a multitude of mechanisms.

The relationship between TMB, risk score, and prognosis

TMB reflects the stability, proliferative capacity, and differentiation level of tumor cells by calculating the number of gene mutations within them. As depicted in *Figure 6A*,*6B*, a significant disparity in TMB was found between the two risk subgroups (P=0.001), with a positive correlation between TMB and risk scores. Notably, the genes *KRAS*, *TP53*, *SMAD4*, *CDKN2A*, and *TTN* harbor a higher frequency of mutations across both groups, with *KRAS* mutations being especially pronounced (*Figure 6C*,*6D*). To further investigate the association between TMB and patient prognosis, PAAD patients were divided into high- and low-TMB groups, followed by Kaplan-Meier survival analysis. The results, as shown in *Figure 6E*, reveal a significant disparity in OS between these groups (P=0.01). Upon integrating the risk scores into our analysis, it was found that patients with both high TMB and high-risk scores exhibited the poorest prognosis, whereas those with low TMB and low-risk scores experienced better OS (*Figure 6F*, P<0.001). The study highlights that individuals classified within the high-risk group tend to have an elevated TMB, and this increased TMB is correlated with a poor prognosis for patients suffering from PAAD.

Analysis of immune-related characteristics in the two groups

Bar plots evaluated the distribution of various immune cell types within PAAD patients (Figure S4A). Correlation heatmaps illustrated the relationships among different immune cell populations (Figure S4B). ssGSEA revealed pronounced differences in the enrichment scores for $CD8^+$ T cells, Mast cells, T helper cells, and tumor-infiltrating lymphocytes (TILs), with higher scores predominantly observed in the low-risk group (*Figure 7A*). It is noteworthy that, among the scores for 13 immune mechanisms, the low-risk group consistently showed higher scores, particularly in chemokine receptor (CCR) signaling, human leukocyte antigen (HLA) presentation, T cell co-stimulation, and type II IFN response (*Figure 7B*). Analysis of immune cell infiltration indicated significant differences in the levels of seven immune cell types between the two risk subgroups. In the high-risk group, there was an increased expression of M0 and M1 macrophages, whereas the low-risk group exhibited a higher prevalence of $CD8^+$ T cells and resting $CD4^+$ memory T cells (*Figure 7C*). Bubble plots depicted the relationship between risk scores and immune cell infiltration using various algorithms (Figure S4C). The analysis revealed that most immune checkpoint proteins were markedly upregulated in the low-risk group,

Copyright © 2025 AME Publishing Company. All rights reserved.

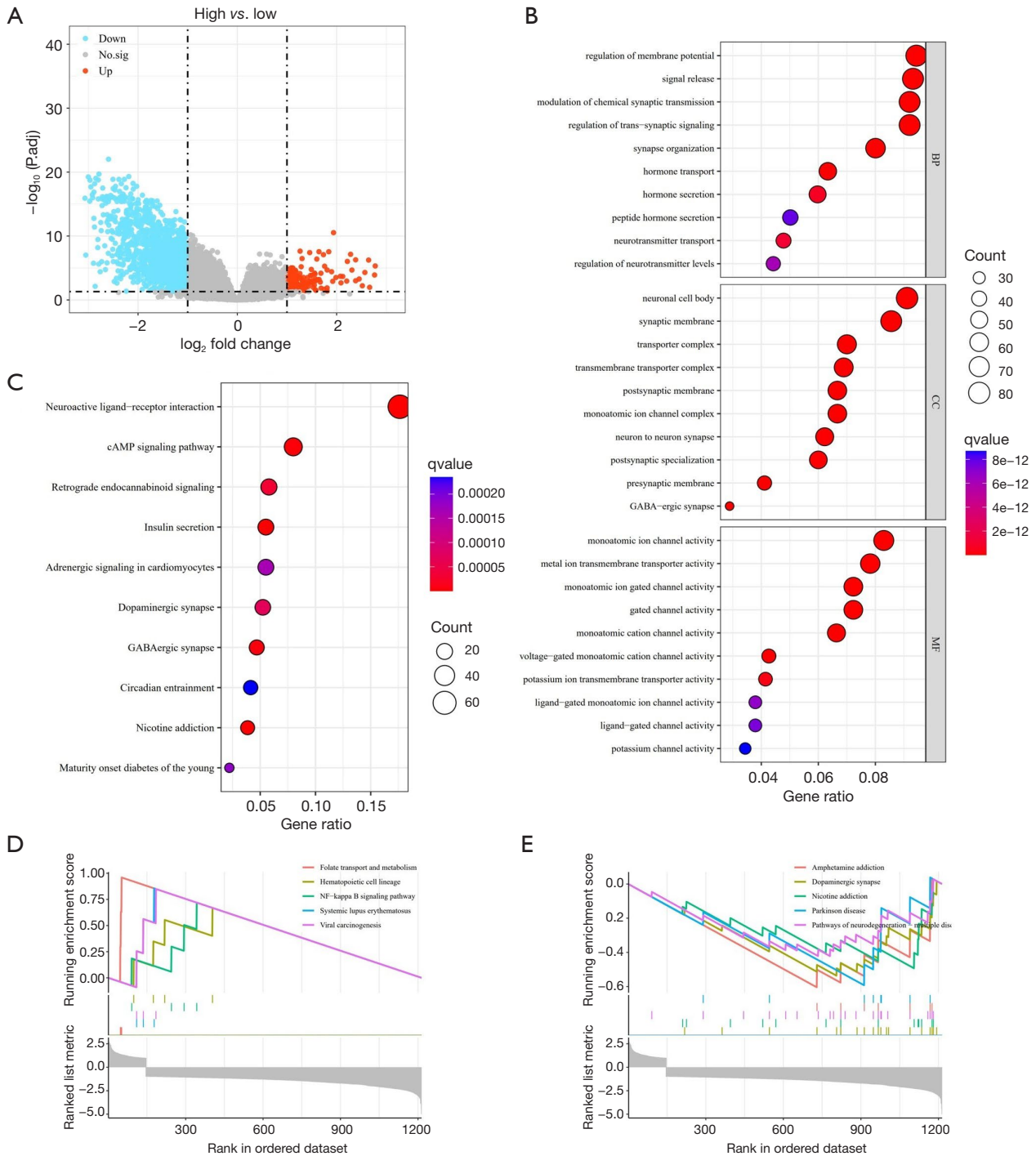


Figure 5 Functional analysis in different risk subgroups. (A) Volcano plot of 1,630 differential genes between two risk subgroups. (B) Bubble chart showing gene enrichment in BP, CC, and MF aspects of GO. (C) KEGG enrichment analysis. GSEA pathway enrichment in the high- (D) and low-risk groups (E). BP, biological process; CC, cellular component; GO, Gene Ontology; GSEA, gene set enrichment analysis; KEGG, Kyoto Encyclopedia of Genes and Genomes; MF, molecular function.

Copyright © 2025 AME Publishing Company. All rights reserved.

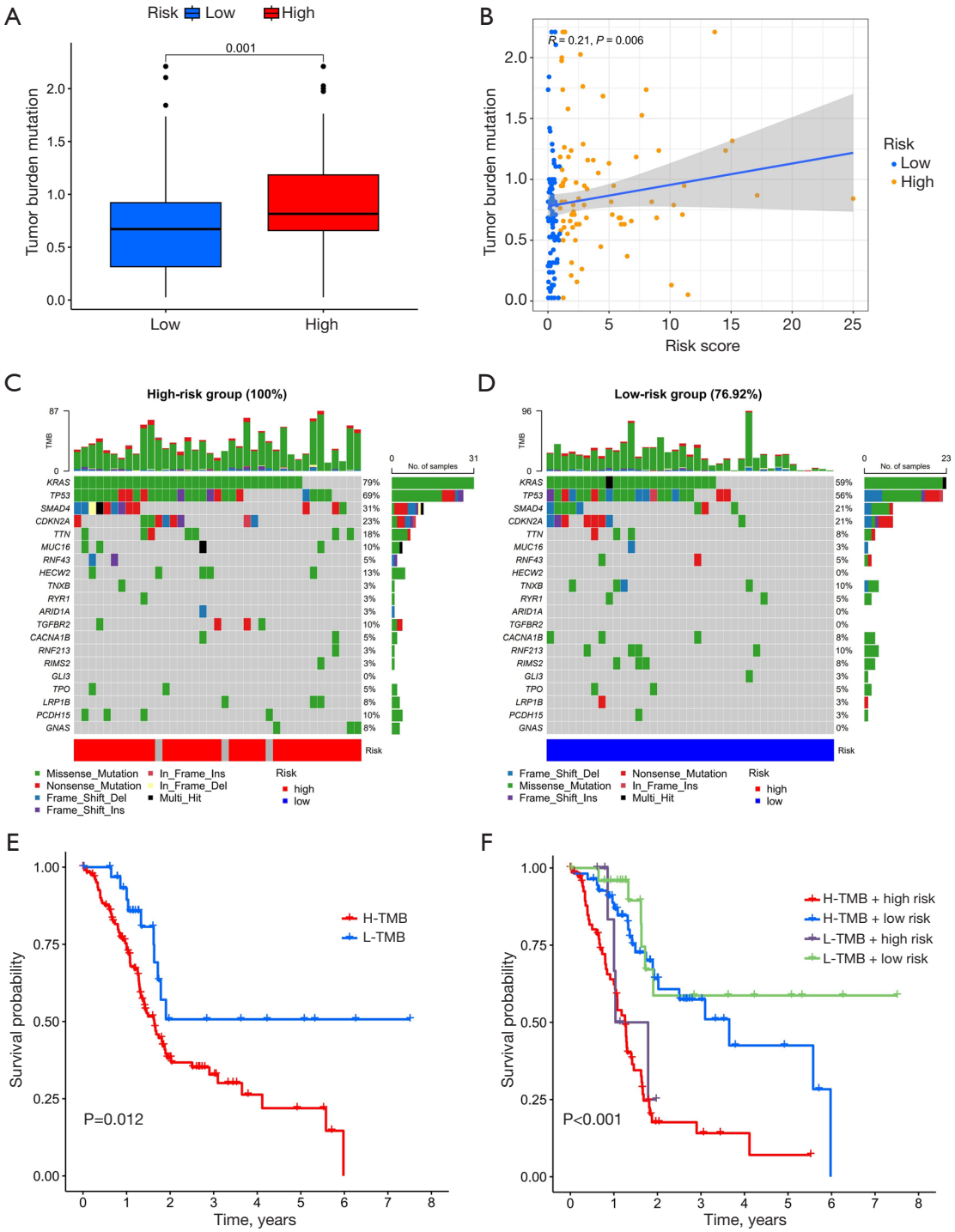


Figure 6 Somatic mutation analysis. (A) Differences in TMB between two risk subgroups. (B) Scatter plot reflecting the correlation between TMB and risk scores. Waterfall plot showing the top 20 mutated genes in high- (C) and low-risk groups (D). (E) Kaplan-Meier survival curves reflecting the survival trends of PAAD patients in high- and low-TMB groups. (F) Kaplan-Meier survival curves of PAAD patients combined with risk scores and TMB as grouping criteria. PAAD, pancreatic adenocarcinoma; TMB, tumor mutational burden.

Copyright © 2025 AME Publishing Company. All rights reserved.

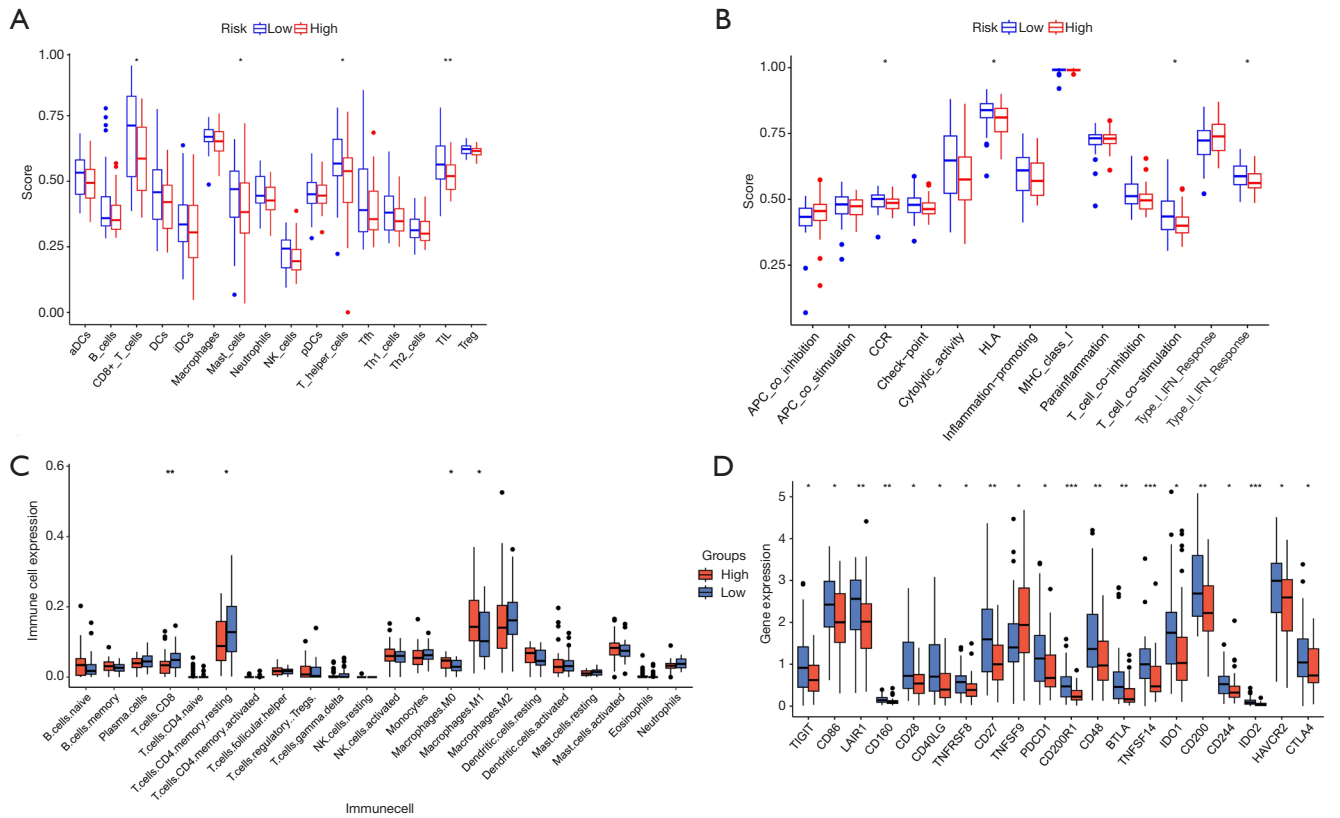


Figure 7 Immune-related analysis. (A,B) ssGSEA analysis of immune cell types and functions. (C) Comparison of immune cell infiltration between two risk subgroups. (D) Expression of immune checkpoints. *, P<0.05; **, P<0.01; ***, P<0.001. ssGSEA, single-sample gene set enrichment analysis.

with TNFSF14 showing the most significant increase in expression (*Figure 7D*). Collectively, these findings suggest that the low-risk group exhibits a more vigorous immune activity within the TME, and immunotherapies targeting immune checkpoints, such as immune checkpoint inhibitors (ICIs), may be particularly effective for this cohort.

Assessment of chemotherapeutic drug efficacy

During the analysis of IC_{50} values for different subgroups of PAAD patients treated with reported clinical drugs, the high-risk group demonstrated greater sensitivity to drugs such as cisplatin and paclitaxel (Figure S5A-S5E), while the low-risk group showed lower IC_{50} values for drugs including Axitinib, Camptothecin, Sunitinib, and Temsirolimus (Figure S5F-S5O). Some of these agents have exhibited tumor-inhibiting properties in clinical trials, suggesting that their combination with existing chemotherapy regimens may potentially enhance therapeutic sensitivity.

Deciphering LINC00705-centered regulatory networks

To delineate the molecular mechanisms underpinning LINC00705-driven pancreatic cancer progression, we established a comprehensive miRNA-mRNA regulatory network through multi-stage bioinformatic interrogation. Intersection analysis of predictions from three independent software tools (miRanda, RNAhybrid, and PITA) identified 47 high-confidence miRNAs potentially interacting with LINC00705, as cataloged in Table S2 and visualized through Venn analysis in Figure S6A. Subsequent validation using four computational modules (microT-CDS, miRmap, PITA, and TargetScan) within the ENCORI database revealed 367 consensus target genes regulated by these miRNAs, with intersection patterns detailed in https://cdn.amegroups.cn/static/public/tcr-2025-582-1.xlsx and Figure S6B. KEGG pathway enrichment analysis of these target genes demonstrated significant enrichment in key oncogenic pathways, dominated by pathways in cancer,

Copyright © 2025 AME Publishing Company. All rights reserved.

PI3K-Akt signaling, microRNAs in cancer, MAPK signaling and mTOR signaling, collectively illustrated in Figure S6C. These findings position LINC00705 as a pivotal regulator that orchestrates cancer-associated signaling axes through miRNA-mediated mRNA targeting, potentially modulating critical cellular processes in PAAD pathogenesis.

Validation of the oncogenic role of LINC00705

Previously, LINC00705 has been implicated in the construction of a gastric cancer-related predictive signature as a disulfidptosis-related lncRNA, achieving good predictive results (32). This suggests that LINC00705 may serve as a potential biomarker for prognostic prediction in gastric cancer. As the TCGA database includes a limited set of normal tissue samples (n=4), which may not accurately reflect the contrast in LINC00705 expression between tumor and normal tissues, we accessed the Gene Expression Profiling Interactive Analysis (GEPIA) platform in an attempt to enhance the reliability of our conclusions by integrating normal tissue samples (n=167) from the Genotype-Tissue Expression Project (GTEx) database for pancreatic cancer to observe the expression levels of LINC00705. We were surprised to find a significant statistical difference in the expression levels of LINC00705 between the two tissues (*Figure 8A*). More importantly, elevated expression levels of LINC00705 were associated with shorter OS (*Figure 8B*). Consequently, we speculated that the overexpression of LINC00705 may contribute positively to the occurrence and metastasis of PAAD. Further investigation into this gene could pave the way for novel therapeutic approaches in treating pancreatic cancer.

Through cellular transfection, we successfully knocked down and overexpressed LINC00705 in pancreatic cancer cell lines PANC-1 and MIAPaCa-2, and the efficiency was confirmed by qRT-PCR (*Figure 8C*). Subsequent EdU (*Figure 8D*) and CCK-8 (*Figure 8E*) assays demonstrated that overexpression of LINC00705 significantly promoted the proliferation of both PANC-1 and MIAPaCa-2 cells, likely through its involvement in cell cycle regulation. Moreover, Transwell assays indicated that LINC00705 enhanced cell migration and invasion (*Figure 8F*), a finding important for understanding the mechanisms of tumor metastasis. Scratch wound assays further supported the promotive role of LINC00705 in cell migration (*Figure 8G*). Corresponding statistical graphs showed significant differences (P<0.05) in EdU incorporation (*Figure 8H,8I*) as well as in migration and invasion capabilities measured by Transwell assays (*Figure 8J-8M*) between the two cell lines with knockdown and overexpression of LINC00705.

Discussion

Currently, most anticancer drugs exert their tumor-suppressive effects by inducing apoptosis. However, the continuous clonal replication and the emergence of drug resistance in cancer cells confer resistance to apoptosis, leading to suboptimal therapeutic outcomes (33). Necroptosis, a form of inflammatory cell death, can alert immune cells by releasing secondary messengers, not only activating immune responses to eliminate cancer cells but also enhancing immune memory capacity, thereby providing patients with long-term antitumor efficacy (34). Consequently, immunology-related research based on this cellular process has been increasingly conducted. It is now understood that, within the TME of pancreatic cancer, the abnormally dense stroma, scarcity of effector T cells, and multiple immune-suppressive characteristics render pancreatic cancer less responsive to a significant portion of immunotherapies (35). Previously, a study has quantified and analyzed the extent of ICD following chemotherapy in pancreatic cancer, suggesting that modulation of immunogenic cells could suppress the progression of PAAD (36). Therefore, exploring the role of ICD in pancreatic cancer has become a highly promising direction. In recent years, the abnormal expression levels of numerous lncRNAs documented during cancer cell proliferation and migration suggest their potential involvement in cancer progression through diverse mechanisms (37). Currently, according to the TNM classification of tumors, the American Joint Committee on Cancer (AJCC) categorizes pancreatic cancer into five stages (38). However, the rapid progression of pancreatic cancer limits the specificity of this staging system in reflecting the TME and prognostic outcomes for patients. Therefore, there is an urgent need for more precise biomarkers to guide the clinical treatment of pancreatic cancer, and lncRNAs associated with ICD may become a better choice.

In this study, we identified six lncRNAs: ZEB2-AS1, AC099792.1, LINC01091, LINC02613, AC005304.3, and LINC00705, and constructed a risk signature for pancreatic cancer. This signature exhibited high accuracy in evaluating patient outcomes. Our nomogram, which integrated five clinical parameters with the risk score, significantly improved the precision of personalized prognostic predictions. The ROC curve analysis of the risk score demonstrated its predictive capability, significantly

Copyright © 2025 AME Publishing Company. All rights reserved.

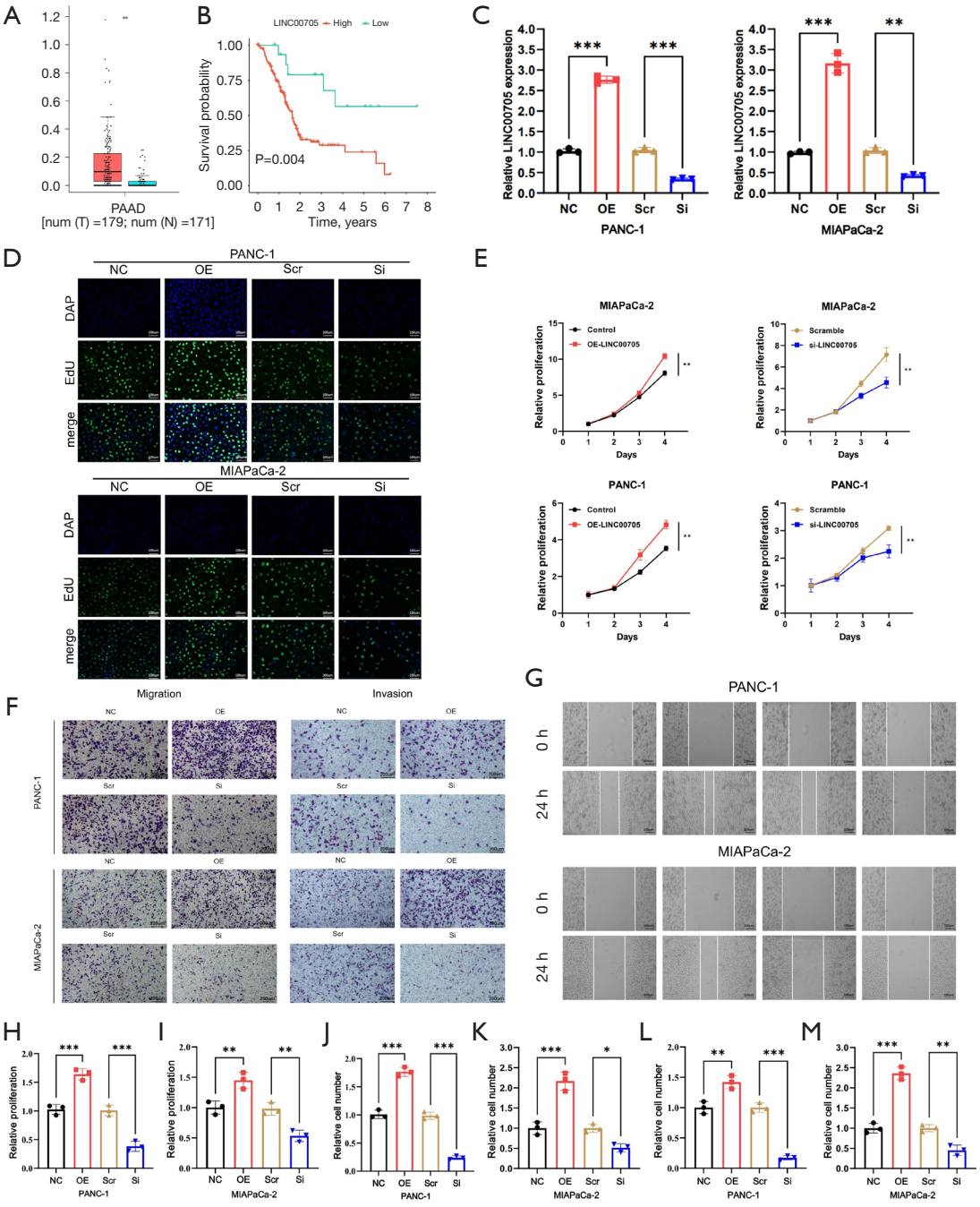


Figure 8 Evaluation and validation of the oncogenic role of LINC00705. (A) Boxplot of LINC00705 expression in PAAD tumor (TCGA, n=179) *vs*. non-tumor tissues [TCGA (n=4) + GTEx (n=167)]. (B) Kaplan-Meier survival curves comparing high/low LINC00705 expression groups. (C) qPCR analysis of LINC00705 in transfected PANC-1 and MIAPaCa-2 cell lines. (D) Representative EdU staining images. (E) CCK-8 assay proliferation curves. (F) Representative Transwell migration assay images. (G) Representative wound healing assay images. (H) Quantitative analysis of EdU+ cells in PANC-1. (I) Quantitative analysis of EdU+ cells in MIAPaCa-2. (J) Transwell migration quantitation in PANC-1. (K) Transwell migration quantitation in MIAPaCa-2. (L) Wound closure rate quantitation in PANC-1. (M) Wound closure rate quantitation in MIAPaCa-2. *, P<0.05; **, P<0.01; ***, P<0.001. CCK-8, Cell Counting Kit-8; EdU, 5-ethynyl-2'-deoxyuridine; GTEx, Genotype-Tissue Expression Project; NC, negative control; OE, overexpression; PAAD, pancreatic adenocarcinoma; qPCR, quantitative polymerase chain reaction; Scr, scrambled control; Si, small interfering; TCGA, The Cancer Genome Atlas.

Copyright © 2025 AME Publishing Company. All rights reserved.

outperforming other clinical features. The scientific validity of this signature was further substantiated by the results of Kaplan-Meier survival analysis, PCA, and time-dependent ROC curve analysis. Besides, we characterized LINC00705, which has been previously implicated as a potential prognostic biomarker for gastric cancer and is positively correlated with tumorigenesis (32). Our findings further support LINC00705 as a promising candidate for guiding treatment strategies in PAAD.

Moreover, GSEA was utilized to uncover the molecular processes involved in the progression of pancreatic cancer. Interestingly, the high-risk group exhibited significant activation of the NF-κB signaling pathway, suggesting a potential oncogenic mechanism. Prior research has reported that NF-κB pathway activation can enhance the expression of cell cycle regulators, such as cyclin D1, thereby promoting pancreatic cancer cell proliferation (39). Concurrently, the team has posited that aberrant activation of the NF-κB pathway may suppress the function of T cells. Consistent with the immune cell infiltration analysis in this study, the TME in the high-risk group had lower infiltration levels of $CD8^+$ T cells, which play a primary cytotoxic role in immune responses, significantly different from the low-risk group. Furthermore, Shang *et al.* (40) suggested that Th cells can assist in the stimulation and growth of immune cells, including $CD8^+$ T cells, through the secretion of cytokines like IFN-γ and interleukin-2 (IL-2). They also create an environment conducive to the activation and function of immune cells by promoting inflammatory responses. Interestingly, compared to the high-risk group, ssGSEA analysis revealed a higher Th cell and $CD8^+$ T cell infiltration in the low-risk group, aligning with previous findings. These observations suggest that the inferior survival outcomes of high-risk patients may be linked to aberrant NF-κB pathway activation. By impairing the function of critical cytotoxic T cells, this physiological process may predominantly weaken the immune response against tumors. Additionally, the functional efficacy of Th cells, $CD8^+$ T cells, and their synergistic anti-tumor effects may be compromised in high-risk patients, hindering their ability to induce ICD and limiting the effectiveness of immunotherapy strategies that rely on autoimmunity. Critically, the ICD-associated lncRNA signature remodels the immunosuppressive PAAD microenvironment through coordinated regulation of cytokine networks and signaling cascades. The enhanced CCR signaling and type II IFN response in low-risk patients are mechanistically linked to lncRNA-mediated upregulation of chemokine axes (e.g., CXCL9/10-CXCR3), which facilitate spatial navigation of cytotoxic lymphocytes through dense stromal barriers—a process essential for T-cell infiltration and tumor antigen recognition (41). Concurrently, attenuation of transforming growth factor-β (TGF-β) signaling pathways disrupts immunosuppressive circuitry by inhibiting Treg differentiation and M2 macrophage polarization, thereby preserving effector T-cell functionality (42). This aligns with the observed reduction in immunosuppressive cells and elevated $CD8^+$ T-cell fractions. Notably, the dysregulated NF-κB activation in high-risk patients contrasts with lncRNA-guided optimization of non-canonical NF-κB pathways in low-risk group, which promotes co-stimulatory molecule expression (e.g., TNFSF14) to balance immune checkpoint activity (43). Such coordinated regulation of chemokine gradients, immunosuppressive pathways, and checkpoint signals establishes an immunogenic niche that enhances ICD induction. The superior immunotherapy response in low-risk patients likely stems from this lncRNA-orchestrated immune remodeling, where synchronized cytokine networks (particularly IL-2/IFN-γ) sustain T-cell proliferation and NK cell activation—ultimately overcoming the autoimmune resistance characteristic of PAAD (44).

In the therapeutic management of cancer, the selection of drug regimens constitutes an essential component of a comprehensive treatment strategy. The higher expression of immune checkpoints in the low-risk group suggests they may derive more significant benefit from treatment with ICIs. Within the armamentarium of first-line chemotherapeutic agents for PAAD, paclitaxel and cisplatin have demonstrated heightened sensitivity in the high-risk patient cohort. Yang *et al.* have documented that paclitaxel facilitates antigen presentation by DCs and induces ICD, thereby augmenting the potency of immune responses by promoting DAMPs release (e.g., ATP and calreticulin) and enhancing phagocytic activity of antigen-presenting cells (45). Notably, a recent phase Ib trial (PANTAX, NCT04652205) further demonstrated that nab-paclitaxel synergizes with DNA-damaging agents like cisplatin by amplifying endoplasmic reticulum stress and surface exposure of calreticulin, key hallmarks of ICD, in pancreatic cancer models (46). The differential sensitivity to these ICD-inducing agents in our high-risk group may be attributed to the regulatory role of ICD-associated lncRNAs (e.g., modulating ER stress sensors such as PERK or DAMPs trafficking), thereby potentiating chemotherapy-induced immunogenicity. Additionally, paclitaxel has been shown to upregulate the expression of the immune

Copyright © 2025 AME Publishing Company. All rights reserved.

checkpoint protein programmed death-ligand 1 (PD-L1), potentially dampening the immune response within the patient (47). These insights lay the theoretical groundwork for the clinical benefits of combining paclitaxel with ICIs and suggest that the meticulous adjustment of dosages and administration schedules for this combinatorial therapy could be instrumental in treating a broader spectrum of cancer types and stages. In the low-risk group, Bcl-2 inhibitors ABT-263 and TW.37 have displayed lower IC_{50} values. Although these compounds have not yet been incorporated into standard clinical oncological practice, evidence from a study indicates that taxane drugs can inhibit the CXCR2/BCL-2 axis, enhancing the sensitivity of prostate cancer (PC) to cisplatin (48). Critically, the synergy between Bcl-2 inhibitors and ICD-associated lncRNAs may originate from their shared modulation of mitochondrial apoptosis pathways. As demonstrated by Cheng *et al.* (2023), Bcl-2 inhibition in low-immune-risk PAAD subsets promotes cytochrome c release, which not only triggers caspase activation but also synergizes with ICD-lncRNAs to amplify DAMPs release (e.g., HMGB1), thereby converting apoptotic cell death into ICD (49). Consequently, we posit that the synergistic administration of Bcl-2 inhibitors, Paclitaxel, and Cisplatin may offer a promising therapeutic combination in oncology, expanding the repertoire of treatment options for pancreatic cancer.

Our mechanistic dissection of the LINC00705-centered regulatory network revealed significant enrichment of its target genes in fundamental oncogenic pathways, most notably pathways in cancer, underscoring its broad relevance to carcinogenesis. Notably, three well-characterized signaling axes—PI3K-Akt, MAPK, and mTOR—emerged as the most significantly enriched pathways. The PI3K-Akt pathway, serving as a pivotal hub governing cell survival, proliferation, and metabolism, exhibits >60% frequency of aberrant activation in PAAD. It confers chemoresistance by suppressing pro-apoptotic Bim and upregulating anti-apoptotic molecules (e.g., BCL-2), thereby attenuating chemotherapy-induced cell death. A previous study further demonstrated that circRNA cFAM124A potentiates gemcitabine resistance in the AG regimen (nab-paclitaxel/gemcitabine) through cathepsin L (CTSL)-mediated generation of truncated tRXRα, which hyperactivates PI3K/Akt signaling (50). Concurrently, the MAPK pathway regulates cell differentiation and proliferation across multiple malignancies (e.g., colorectal cancer, melanoma) (51,52). In PAAD, single-agent inhibition of KRAS-MAPK signaling triggers compensatory HER2 phosphorylation and drug resistance. Strikingly, combinatorial therapy with MAPK inhibitors (ulixertinib or trametinib) and the HER2-targeting antibody-drug conjugate trastuzumab deruxtecan (DS-8201a) achieves near-complete tumor regression (>90% volume reduction) in patient-derived xenograft (PDX) models with favorable tolerability (53), establishing MAPK's central role in adaptive resistance. As a key downstream effector of PI3K-Akt, mTORC1 orchestrates metabolic reprogramming by integrating nutrient signals. mTORC1 activation induces SREBP1-dependent transcription of stearoyl-CoA desaturase-1 (SCD1), promoting fatty acid desaturation and lipid droplet accumulation to sustain anabolic metabolism while inhibiting ferroptosis in PAAD cells (50). Consequently, LINC00705 may synergistically amplify oncogenic signaling flux through coordinated targeting of critical nodes, ultimately potentiating metabolic plasticity, therapy resistance, and metastatic competence in pancreatic cancer.

In this investigation, we pioneered the development of a novel prognostic signature based on lncRNAs associated with ICD. The efficacy and reliability of this signature were rigorously validated by correlating it with the survival data of a cohort of pancreatic cancer patients. Subsequently, we integrated the risk scores derived from this signature with the clinical parameters of pancreatic cancer patients to construct ROC curves and nomograms. Our findings are particularly noteworthy considering the aggressive nature of pancreatic cancer and the limitations of traditional staging methods in accurately predicting patient outcomes. The rapid progression of cancer cells often outpaces the discriminatory power of clinical staging (AUC =0.492), necessitating a more comprehensive approach to prognostic assessment. Furthermore, our comprehensive analysis of TMB and immune-related factors revealed that patients classified as low-risk based on our signature exhibit heightened immune responsiveness, suggesting potential targets for immunotherapeutic interventions. The predictive capabilities of our signature extend to the anticipation of chemotherapeutic drug sensitivity, offering a valuable tool for optimizing multimodal treatment strategies for pancreatic cancer. A series of *in vitro* experiments have highlighted the pivotal role of LINC00705 as a key regulatory molecule in cellular behavior, particularly within the context of oncology. These findings suggest that LINC00705 may emerge as a promising therapeutic target for pancreatic cancer. However, this study is not without limitations. Initially, the availability of comprehensive clinical data for pancreatic cancer patients across various

Copyright © 2025 AME Publishing Company. All rights reserved.

databases is limited, and even within the TCGA database, the number of normal tissue samples remains relatively small. This poses a challenge to the stability of our predictive model and its external validation. Additionally, the sample size for patients in stage III and stage IV is relatively small, which may compromise the scoring accuracy for the 'Stage' factor during the construction of the nomogram. Lastly, while our *in vitro* experiments have implicated the overexpression of LINC00705 as a potential adverse prognostic indicator in pancreatic cancer patients, the underlying molecular mechanisms remain to be fully elucidated.

Conclusions

The prognostic signature constructed based on six ICD-associated lncRNAs demonstrates a high degree of predictive accuracy. Within the low-risk cohort, the mechanisms underlying immunotherapy are intricately linked to T cells and the T cell receptor signaling pathways they initiate. Our analysis suggests that Bcl-2 inhibitors may hold substantial promise in the advancement of future therapeutics. Additionally, LINC00705's facilitative role in various biological behaviors of pancreatic cancer cells positions it as a viable target for pancreatic cancer.

Acknowledgments

The authors sincerely thank all participants in this study.

Footnote

Reporting Checklist: The authors have completed the TRIPOD and MDAR reporting checklists. Available at https://tcr.amegroups.com/article/view/10.21037/tcr-2025-582/rc

Data Sharing Statement: Available at https://tcr.amegroups.com/article/view/10.21037/tcr-2025-582/dss

Peer Review File: Available at https://tcr.amegroups.com/article/view/10.21037/tcr-2025-582/prf

Funding: This study was supported by the National Nature Science Foundation of China (No. 82203735) and Gusu Health Talent Program (No. GSWS2022026).

Conflicts of Interest: All authors have completed the ICMJE uniform disclosure form (available at https://tcr.amegroups.com/article/view/10.21037/tcr-2025-582/coif). The authors have no conflicts of interest to declare.

Ethical Statement: The authors are accountable for all aspects of the work in ensuring that questions related to the accuracy or integrity of any part of the work are appropriately investigated and resolved. The study was conducted in accordance with the Declaration of Helsinki and its subsequent amendments. Ethical approval was obtained from the Ethics Committee of The First Affiliated Hospital of Soochow University (No. 2025742). Informed consent was exempted as all patient data were derived from deidentified public databases where original ethical compliance had been established.

Open Access Statement: This is an Open Access article distributed in accordance with the Creative Commons Attribution-NonCommercial-NoDerivs 4.0 International License (CC BY-NC-ND 4.0), which permits the non-commercial replication and distribution of the article with the strict proviso that no changes or edits are made and the original work is properly cited (including links to both the formal publication through the relevant DOI and the license). See: https://creativecommons.org/licenses/by-nc-nd/4.0/.

References

1. Cai J, Chen H, Lu M, et al. Advances in the epidemiology of pancreatic cancer: Trends, risk factors, screening, and prognosis. Cancer Lett 2021;520:1-11.
2. Ferlay J, Colombet M, Soerjomataram I, et al. Cancer incidence and mortality patterns in Europe: Estimates for 40 countries and 25 major cancers in 2018. Eur J Cancer 2018;103:356-87.
3. Advancing on pancreatic cancer. Nat Rev Gastroenterol Hepatol 2021;18:447.
4. Schneider M, Hackert T, Strobel O, et al. Technical advances in surgery for pancreatic cancer. Br J Surg 2021;108:777-85.
5. Truty MJ, Kendrick ML, Nagorney DM, et al. Factors Predicting Response, Perioperative Outcomes, and Survival Following Total Neoadjuvant Therapy for Borderline/Locally Advanced Pancreatic Cancer. Ann Surg 2021;273:341-9.
6. Schizas D, Charalampakis N, Kole C, et al. Immunotherapy for pancreatic cancer: A 2020 update. Cancer Treat Rev 2020;86:102016.

Copyright © 2025 AME Publishing Company. All rights reserved.

7. Ho WJ, Jaffee EM, Zheng L. The tumour microenvironment in pancreatic cancer - clinical challenges and opportunities. Nat Rev Clin Oncol 2020;17:527-40.
8. Ahmed A, Tait SWG. Targeting immunogenic cell death in cancer. Mol Oncol 2020;14:2994-3006.
9. Gong T, Liu L, Jiang W, et al. DAMP-sensing receptors in sterile inflammation and inflammatory diseases. Nat Rev Immunol 2020;20:95-112.
10. Paludan SR, Reinert LS, Hornung V. DNA-stimulated cell death: implications for host defence, inflammatory diseases and cancer. Nat Rev Immunol 2019;19:141-53.
11. West AP, Shadel GS. Mitochondrial DNA in innate immune responses and inflammatory pathology. Nat Rev Immunol 2017;17:363-75.
12. Fucikova J, Kepp O, Kasikova L, et al. Detection of immunogenic cell death and its relevance for cancer therapy. Cell Death Dis 2020;11:1013.
13. Wang Y, Yang R, Xie Y, et al. Comprehensive review of drug-mediated ICD inhibition of breast cancer: mechanism, status, and prospects. Clin Exp Med 2024;24:230.
14. Kroemer G, Kepp O. Small cell lung cancer responds to immunogenic chemotherapy followed by PD-1 blockade. Oncoimmunology 2021;10:1996686.
15. Bridges MC, Daulagala AC, Kourtidis A. LNCcation: lncRNA localization and function. J Cell Biol 2021;220:e202009045.
16. Arora R, Lee Y, Wischnewski H, et al. RNaseH1 regulates TERRA-telomeric DNA hybrids and telomere maintenance in ALT tumour cells. Nat Commun 2014;5:5220.
17. Kleaveland B, Shi CY, Stefano J, et al. A Network of Noncoding Regulatory RNAs Acts in the Mammalian Brain. Cell 2018;174:350-362.e17.
18. Ballarino M, Morlando M, Fatica A, et al. Non-coding RNAs in muscle differentiation and musculoskeletal disease. J Clin Invest 2016;126:2021-30.
19. Li JR, Liu L, Luo H, et al. Long Noncoding RNA DUXAP8 Promotes Pancreatic Carcinoma Cell Migration and Invasion Via Pathway by miR-448/WTAP/Fak Signaling Axis. Pancreas 2021;50:317-26.
20. Wang Y, Li X, Huang Y, et al. The Prognostic Value and Potential Immune Mechanisms of lncRNAs Related to Immunogenic Cell Death in Papillary Thyroid Carcinoma. J Inflamm Res 2024;17:1995-2008.
21. Shu K, Cai C, Chen W, et al. Prognostic value and immune landscapes of immunogenic cell death-associated lncRNAs in lung adenocarcinoma. Sci Rep 2023;13:19151.
22. Anders S, Huber W. Differential expression analysis for sequence count data. Genome Biol 2010;11:R106.
23. Mandrekar JN. Receiver operating characteristic curve in diagnostic test assessment. J Thorac Oncol 2010;5:1315-6.
24. Wang J, Qin D, Tao Z, et al. Identification of cuproptosis-related subtypes, construction of a prognosis model, and tumor microenvironment landscape in gastric cancer. Front Immunol 2022;13:1056932.
25. Wu J, Zhang H, Li L, et al. A nomogram for predicting overall survival in patients with low-grade endometrial stromal sarcoma: A population-based analysis. Cancer Commun (Lond) 2020;40:301-12.
26. Xenopoulos P, Rulff J, Nonato LG, et al. Calibrate: Interactive Analysis of Probabilistic Model Output. IEEE Trans Vis Comput Graph 2023;29:853-63.
27. Kanehisa M, Goto S. KEGG: kyoto encyclopedia of genes and genomes. Nucleic Acids Res 2000;28:27-30.
28. Hänzelmann S, Castelo R, Guinney J. GSVA: gene set variation analysis for microarray and RNA-seq data. BMC Bioinformatics 2013;14:7.
29. Cui Y, Chen H, Xi R, et al. Whole-genome sequencing of 508 patients identifies key molecular features associated with poor prognosis in esophageal squamous cell carcinoma. Cell Res 2020;30:902-13.
30. Heo G, Gader P, Frigui H. RKF-PCA: robust kernel fuzzy PCA. Neural Netw 2009;22:642-50.
31. Chen Y, Feng Y, Yan F, et al. A Novel Immune-Related Gene Signature to Identify the Tumor Microenvironment and Prognose Disease Among Patients With Oral Squamous Cell Carcinoma Patients Using ssGSEA: A Bioinformatics and Biological Validation Study. Front Immunol 2022;13:922195.
32. Kang K, Li X, Peng Y, et al. Comprehensive Analysis of Disulfidptosis-Related LncRNAs in Molecular Classification, Immune Microenvironment Characterization and Prognosis of Gastric Cancer. Biomedicines 2023;11:3165.
33. Mosca L, Ilari A, Fazi F, et al. Taxanes in cancer treatment: Activity, chemoresistance and its overcoming. Drug Resist Updat 2021;54:100742.
34. Meier P, Legrand AJ, Adam D, et al. Immunogenic cell death in cancer: targeting necroptosis to induce antitumour immunity. Nat Rev Cancer 2024;24:299-315.
35. Riquelme E, Maitra A, McAllister F. Immunotherapy for Pancreatic Cancer: More Than Just a Gut Feeling. Cancer Discov 2018;8:386-8.
36. Ye J, Mills BN, Zhao T, et al. Assessing the Magnitude of Immunogenic Cell Death Following Chemotherapy and

Copyright © 2025 AME Publishing Company. All rights reserved.

Irradiation Reveals a New Strategy to Treat Pancreatic Cancer. Cancer Immunol Res 2020;8:94-107.
37. Bin Wang, Yuan C, Qie Y, et al. Long non-coding RNAs and pancreatic cancer: A multifaceted view. Biomed Pharmacother 2023;167:115601.
38. Kolbeinsson HM, Chandana S, Wright GP, et al. Pancreatic Cancer: A Review of Current Treatment and Novel Therapies. J Invest Surg 2023;36:2129884.
39. Pramanik KC, Makena MR, Bhowmick K, et al. Advancement of NF-κB Signaling Pathway: A Novel Target in Pancreatic Cancer. Int J Mol Sci 2018;19:3890.
40. Shang Q, Yu X, Sun Q, et al. Polysaccharides regulate Th1/Th2 balance: A new strategy for tumor immunotherapy. Biomed Pharmacother 2024;170:115976.
41. Chen SY, Kung HC, Espinoza B, et al. Distinct response to IL-1β blockade in liver- and lung-specific metastasis mouse models of pancreatic cancer with heterogeneous tumor microenvironments. Exp Hematol Oncol 2025;14:13.
42. Shi M, Zhang R, Lyu H, et al. Long non-coding RNAs: Emerging regulators of invasion and metastasis in pancreatic cancer. J Adv Res 2025;S2090-1232(25)00073-6.
43. Jasim SA, Pallathadka H, Hjazi A, et al. LncRNA-Histone Modification Crosstalk: Orchestrating Cancer Pathobiology. Naunyn Schmiedebergs Arch Pharmacol 2025. [Epub ahead of print]. doi: 10.1007/s00210-025-04402-6.
44. Zhang X, Lao M, Yang H, et al. Targeting cancer-associated fibroblast autophagy renders pancreatic cancer eradicable with immunochemotherapy by inhibiting adaptive immune resistance. Autophagy 2024;20:1314-34.
45. Yang Q, Shi G, Chen X, et al. Nanomicelle protects the immune activation effects of Paclitaxel and sensitizes tumors to anti-PD-1 Immunotherapy. Theranostics 2020;10:8382-99.
46. Shim S, Reinacher-Schick A, Kraeft AL, et al. PANTAX: a phase Ib clinical trial of the efflux pump inhibitor SCO-101 in combination with gemcitabine and nab-paclitaxel in non-resectable or metastatic pancreatic cancer. Invest New Drugs 2025;43:337-47.
47. Serpico AF, Pisauro C, Grieco D. cGAS-dependent proinflammatory and immune homeostatic effects of the microtubule-targeting agent paclitaxel. Front Immunol 2023;14:1127623.
48. Ruiz de Porras V, Wang XC, Palomero L, et al. Taxane-induced Attenuation of the CXCR2/BCL-2 Axis Sensitizes Prostate Cancer to Platinum-based Treatment. Eur Urol 2021;79:722-33.
49. Cheng D, Hu J, Wu X, et al. PD-1 blockade combined with gemcitabine plus nab-paclitaxel is superior to chemotherapy alone in the management of unresectable stage III/IV pancreatic cancer: a retrospective real-world study. Front Oncol 2023;13:1281545.
50. Cao Y, Wang X, Liu Y, et al. BHLHE40 Inhibits Ferroptosis in Pancreatic Cancer Cells via Upregulating SREBF1. Adv Sci (Weinh) 2024;11:e2306298.
51. Huang P, Ji F, Cheung AH, et al. Peptostreptococcus stomatis promotes colonic tumorigenesis and receptor tyrosine kinase inhibitor resistance by activating ERBB2-MAPK. Cell Host Microbe 2024;32:1365-1379.e10.
52. Huang F, Cai F, Dahabieh MS, et al. Peroxisome disruption alters lipid metabolism and potentiates antitumor response with MAPK-targeted therapy in melanoma. J Clin Invest 2023;133:e166644.
53. Bulle A, Liu P, Seehra K, et al. Combined KRAS-MAPK pathway inhibitors and HER2-directed drug conjugate is efficacious in pancreatic cancer. Nat Commun 2024;15:2503.

Cite this article as: Zhu H, Gan X, Shen D, Sun D. Deciphering immune landscapes: an ICD-lncRNA-derived prognostic signature for pancreatic adenocarcinoma. Transl Cancer Res 2025;14(10):7256-7276. doi: 10.21037/tcr-2025-582

Copyright © 2025 AME Publishing Company. All rights reserved.